

Microstructural and Mechanical Properties Evaluation of Tungsten Inert Gas-Welded 316 Stainless Steel and Pure Copper Joint

**Naveen Thomas, A. Mathew, Kurias
George, Noble Thomas, Sherin Thampi,
Akash Biradar & M. Rijesh**

**Metallography, Microstructure, and
Analysis**

Application and Innovation for Metals,
Alloys, and Engineered Materials

ISSN 2192-9262

Metallogr. Microstruct. Anal.
DOI 10.1007/s13632-020-00682-x



Your article is protected by copyright and all rights are held exclusively by ASM International. This e-offprint is for personal use only and shall not be self-archived in electronic repositories. If you wish to self-archive your article, please use the accepted manuscript version for posting on your own website. You may further deposit the accepted manuscript version in any repository, provided it is only made publicly available 12 months after official publication or later and provided acknowledgement is given to the original source of publication and a link is inserted to the published article on Springer's website. The link must be accompanied by the following text: "The final publication is available at link.springer.com".



Microstructural and Mechanical Properties Evaluation of Tungsten Inert Gas-Welded 316 Stainless Steel and Pure Copper Joint

Naveen Thomas¹ · A. Mathew¹ · Kurias George¹ · Noble Thomas¹ · Sherin Thampi¹ · Akash Biradar² · M. Rijesh³

Received: 22 May 2020 / Revised: 9 September 2020 / Accepted: 10 September 2020
© ASM International 2020

Abstract

Tungsten inert gas welding of 316 stainless steel and 99.9% pure copper using nickel as filler metal was performed. The optimized process parameters adapted for the welding process are described. The microstructural studies revealed a complex heterogeneous fusion zone microstructures characterized both by rapid cooling and poor mixing of the materials which contain main elements which are mutually insoluble. Also, the welded specimen did not expose any defects such as porosity and cracks; however, some copper diffusion through the grain boundaries of steel was observed at the steel and fusion zone interface. The microhardness shows homogeneous values at the weld root and a higher hardness with more inhomogeneity at the weld face. The tensile strength of the weld sample was measured to be 143.7 MPa.

Keywords TIG welding · Copper · 316 stainless steel · Dissimilar joint · SEM

Introduction

The consolidation of the diversified properties of dissimilar materials has significant dominance over the performance-based materials in modern industrial sectors. Welding of dissimilar metals pursues various advantages for combining and obtaining the constructive properties of two different metals or alloys. As being capable of obtaining material with multiple metallurgical and mechanical properties, the dissimilar metal joining processes have acquired considerable attention during the recent years [1, 2]. However, the various researches in this field reveal that the welding of dissimilar metals is challenging. This is mainly associated with the mutual solubility among the material to be welded [3]. Moreover, during fusion welding, the filler metal used should be soluble in each of the base metal to be welded.

The thermal expansion coefficients of base metal need to be compatible to avoid thermal fatigue. Hence, it is challenging to join the metal and alloys with diverse melting points and thermal conductivities [4, 5]. Despite of this, many joining processes were developed, such as electron beam welding (EBW) [6], Magnetic pulse welding (MPW) [7], laser beam welding (LBM) [8], diffusion bonding, explosive cladding (EC) [9], friction welding (FW) [10], roll bonding (RB) [11], tungsten inert gas welding (TIG), and shielded metal arc welding (SMAW).

Stainless steel is a very important engineering material with essential structural need. Combining stainless steel with copper serves many purposes in industrial and structural applications. Copper has many attractive properties including considerable deformability, high thermal and electrical conductivity, and machinability. However, the applications of copper-alloys were constrained due to its high cost and higher specific weight. Hence, the partial reinstatement of copper alloy components by ferrous alloys would be an advantageous way. Among all the above-mentioned welding processes, tungsten inert gas welding (TIG) is one of the popular and economical techniques used for the joining of a wide variety of metals and alloys. The technique uses the arc produced at the non-consumable tungsten electrode and the workpiece junction for coalescing the metals. To shield the electrode and molten pool from the contaminant atmosphere, an inert gas is been made to flow over the weld zone. This

✉ M. Rijesh
rijesh.m@vit.ac.in

Akash Biradar
akash.vijaykumar@vit.ac.in

¹ Mechanical Engineering, Amal Jyothi College of Engineering, Kanjirappally, India

² School of Mechanical Engineering, Vellore Institute of Technology, Vellore, India

³ Manufacturing Engineering, VIT Vellore, Vellore, India

technique can achieve a high-quality weldment for stainless steel and many nonferrous alloys [12, 13]. A considerable difference in the melting points as well as thermal conductivities of Cu and steel alloy makes the welding of this combination very difficult possible. One of the two major problems associated with SS-316 and copper welding is that the copper side always persists a coarse grain structure. Another problem is hot cracking in the heat-affected zone of steel, since copper diffuses through the grain boundary of steel [14]. Many efforts were made to investigate the feasibility of welding of steel and copper [15–19]. Magnabosco et al. [18] investigated the fusion zone of copper–stainless steel weldment produced by electron beam welding (EBW) and concluded that the rapid cooling rate and improper mixing of coalescence during welding caused heterogeneous microstructure. Zhang et al. [16] have successfully welded the stainless steel and copper by the EBW technique, using copper wire as filler metal. The study revealed that the microstructure was mainly composed of a dendritic phase (α) with a randomly dispersed globular (δ) phase. However, precise focusing of the beam at the joint line is very difficult under deviating electromagnetic environment. The study of microstructure and properties of friction stir welded Cu-SS joint by Joshi et al. [15] shows a microstructure resembling metal matrix composite with copper as a matrix consisting of randomly dispersed steel particles. It is reported that the extreme recrystallization at the copper side and severe defects during welding at the weld zone are some major limitations causing degradation of joint properties. The same authors investigated the effect of gas tungsten arc welding (GTAW) current on the SS-Cu dissimilar joint formation

and reported that better joint properties with 79% of joint efficiency were obtained at 15A GTAW current [20]. Velu and Bhat [21] investigated the major effect of bronze and nickel filler wires on mechanical and metallurgical properties of steel-copper joints and concluded that the use of nickel-base alloy as the filler material is most suitable for the process. Very limited works were reported on TIG welding of stainless steel and copper. The majority of published researches focused on finding suitable filler metal. Thus, the authors found it worthwhile to investigate the feasibility of TIG welding to join copper and 316 stainless steel and shed some insights on the weld properties of the obtained joint. In the current study, welding is carried out using nickel as filler material based on certain definite parameters.

Experimental Procedure

Commercial purity copper and 316 stainless steel plates of dimension $150 \times 100 \times 5$ mm are selected as base metals. The chemical compositions of both the materials are tabulated in Table 1. Before welding, the base metal plates were cleaned mechanically and chemically using brush and acetone, respectively. Figure 1 illustrates the schematic of the joint configuration used for SS-316 and copper plates. Tungsten inert gas (TIG) welding is performed at constant current supply, using a 2.4 mm diameter nickel filler rod. Table 2 provides optimized welding parameters incorporated in the present work. Homogeneous heat input is provided across both the base metals, in a selected single bevel joint configuration. 45° of bevel geometry are

Table 1 Elemental composition of SS-316 and CP copper

	Elements in wt.%								
	C	Ni	Cr	Si	Mn	S	Mo	Fe	Cu
SS-316	0.08	9.2	18.5	0.45	1.65	0.003	2.7	66.95	0.45
CP Cu	–	0.002	–	–	–	0.002	–	0.095	99.9
ER NiCr-3 wire	0.1	67	22	0.5	2.5	.015	–	–	0.5



Fig. 1 (a) Schematic dimension of weld plates and (b) plates after TIG welding

Table 2 The welding parameters

Parameters	Value
Welding gas	Argon
Welding current	180A
Voltage	17.2 V
Gas flow	7 L/min
Nozzle diameter	5 mm
Welding passes	2
Plate thickness	5 mm
Filler rod diameter	2.4 mm

provided at the copper side to compensate heat loss across the butt line. The copper plate is preheated to 500 °C, as it conducts heat from the weld joint to the surrounding at a faster rate in comparison with the SS-316 [22]. Multi-pass welding is performed, in which the first pass was through the face and the second at the root for compensating lack of penetration.

By using a wire cut electric discharge machine, the weldment was sliced to prepare metallographic and tensile test samples. Five millimeter thick samples with a cross section of 40 mm × 10 mm were cut for optical microscopic studies. The samples are initially subjected to mechanical polishing by 240, 400, 600, 800, 1000, and 1200 grit size emery papers, respectively, followed by final disk polishing. During disk polishing alumina abrasive particle suspended in water and Kemet diamond compound paste are used to remove the metal uniformly from the surface and to obtain mirror finish. To reveal the microstructure, weldment was chemically etched carefully at the butting line; which consists of various zones like heat-affected zone, fusion zone, and parent metal. HCl (25 ml) + FeCl₃ (5gm) + H₂O (100 ml) etchant solution was used at copper side, whereas 5% nital at the stainless steel side. Two-step etching treatment is carried out in the present study. Initially, the SS-316 is etched with a 5% nital solution. While etching the copper side, the SS-316 portion is carefully covered with water-resistant plaster as the ferric chloride content of copper etchant affect the stainless steel surface. The microstructure of various weld zones is observed using an optical microscope (OLYMPUS SZX12) at 100, 200, and 500 magnifications. Furthermore, the intermixing

phenomenon was analyzed using scanning electron microscope (SEM at 2 k magnification) and energy-dispersive X-ray spectroscopy (EDX).

The tensile test specimens of rectangular cross section (transverse tensile specimens) are cut according to the ASTM standard E8/ E8M-09. The gauge length and cross section are 200 mm and 30 mm × 5 mm, respectively. The test is performed using 40-ton capacity universal testing machine at ambient temperature with a constant strain rate of 2 mm/min. To perform Nick Break Test, a transverse specimen of 28 mm × 5 mm is cut and notched across the weld bead. The angle and depth of the notch were 45° and 6.35 mm, respectively. The two ends of the samples are placed on steel supports and using a heavy hammer the specimen was stroked over the transverse section to break. The specimen after the breaking is depicted in Fig. 2b exposing the broken surface. Vickers microhardness is measured across the weld bead of the joint. Two sets of readings were taken one at the weld face and another at weld root. The microhardness test was performed by applying 300 gf load for 10 s dwell time on Matsuzawa MMT-X Vickers hardness tester.

Results and Discussion

Microstructure

The current study emphasizes that TIG welding can be a popular technique to weld SS-316 and copper using nickel wire as a filler material by adjusting the process parameters as provided in Table 2. The broken section of the weldment as a result of the Nick break test as shown in Fig. 2b confirms by visual inspection that there was no evidence of macroscopic cracks at the joint. The microstructural evolution upon joining of dissimilar metals along with the filler material accomplishes a complex phenomenon. Generally, it builds and promotes a heterogeneous structure at the fusion zone, during the solidification of the molten pool. A vast discrepancy in the thermal conductivities of base metals leads to a disparate cooling rate across the weld interface. Hence, in the present study, complex microstructural development was observed at the

Fig. 2 (a) Sample prepared for microstructural study, and b) Nick break test samples



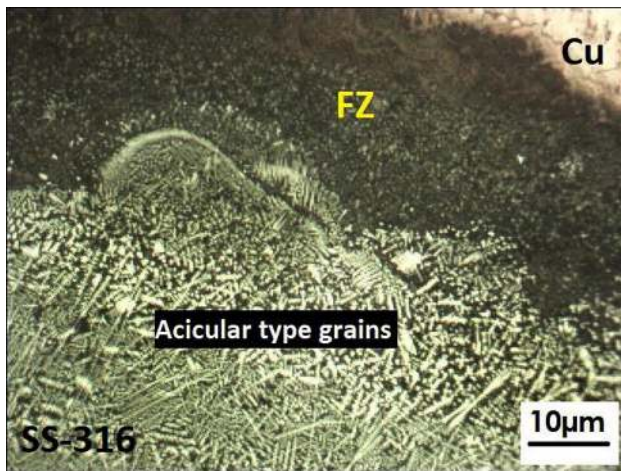


Fig. 3 Acicular type grains at steel fusion zone

weld interface. The optical microscopic image depicted in Fig. 3 shows an acicular morphology of phase, which tends to grow in the perpendicular direction to the weld junction toward the steel. The SEM image (Fig. 4a) shows, a clear SS/weld interface and the heat-affected zone (HAZ) of steel. Also, a large number of lumps of weld metal in fine coronal shaped particles appear at the fusion zone (FZ) and copper interface, (Fig. 5). The dark globular phase (rich in Fe) is found to be embedded depressively in the light zone (rich in Cu), which is in agreement with the previous study conducted by Shiri et al. [22] Further analysis in conjunction with the Fe-Cu phase diagram [23] describes that it is very difficult to form any compound at the fusion zone. Even though Fe has limited solid solubility, i.e., 11.5% Cu in Fe and 3.5% Fe in Cu, it is expected that some precipitated carbides may be latched on the Cu and SS-316 coalescence. Energy-dispersive X-ray analysis (EDAX) conducted at the weld interface, shown in Fig. 4b, reveals the presence of carbides. The

presence of chromium and carbon along with Fe and Cu confirms carbide (chromium carbide) precipitation at the fusion zone. Presumably, some portion of HAZ comprises of solute liquation bands as well as diffusion of SS base metal and Ni filler metal, as shown in Fig. 6. The low thermal diffusivity of SS-316 retains heat across the interface which must have promoted chromium carbide dissolution from the grain boundaries, resulting in a reduction in the amount of chromium and carbon in the base metal. Joshi et al. [15] shown that the increase in heat input imparts ample effect on the solute bands. Moreover, the liquation of the solute band is a function of temperature gradient and solute segregation at the vicinity of the weld interface. The optical micrograph (Fig. 6) reveals the grain coarsening at copper HAZ. The grain coarsening is due to the high thermal conductivity of Cu in comparison with SS-316. The higher thermal conductivity of copper may have also restricted the diffusion of filler metal and SS base into the Cu, and similar results were reported in [24].

The primary epitaxial columnar grain growth followed by secondary dendrites is seen near the interface, shown in (Fig. 7). Furthermore, the cellular structure and the transformed equiaxed columnar dendrites were also observed near the weld face region. The development of coarse-grained microstructures toward the center of the face was due to multi-pass welding. On the other hand, the weld face mid-section revealed cellular structure due to the high heat concentration [25]. Figure 8a, b depicts the Fe-rich phase diffused in the Cu-rich zone. The investigation on Cu-Fe super cooled liquids by Munitz et al. [26] revealed that the sphere-shaped Fe-rich phase originates when the liquid has a lower content of Cu (<50%). The liquation grain boundaries observed in SEM (Fig. 8b) suggest partial melting at the HAZ. This may be due to the multi-pass (two steps) welding. It is found that the presence of high Ni content is susceptible to creating liquation boundaries when subjected to more number of heating and cooling cycles [27].

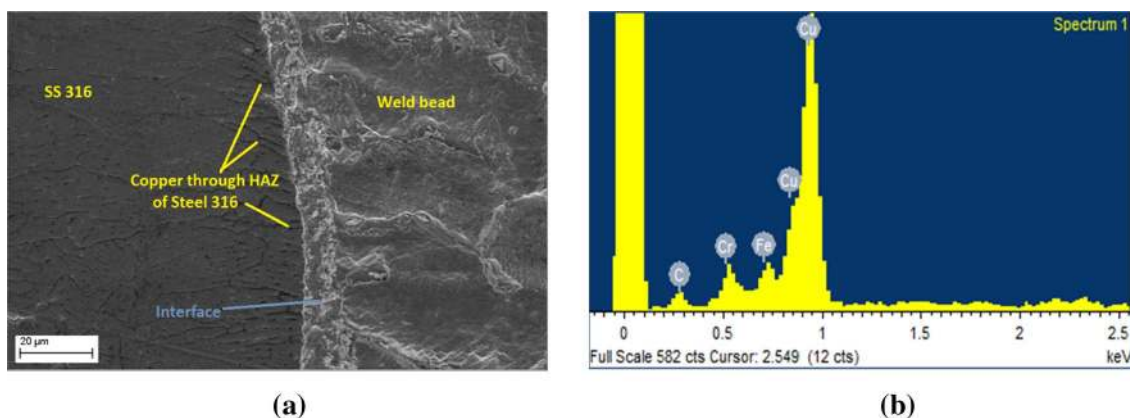


Fig. 4 (a) SEM image showing weld interface and HAZ of SS. (b) EDAX result taken for the same at the interface marked area

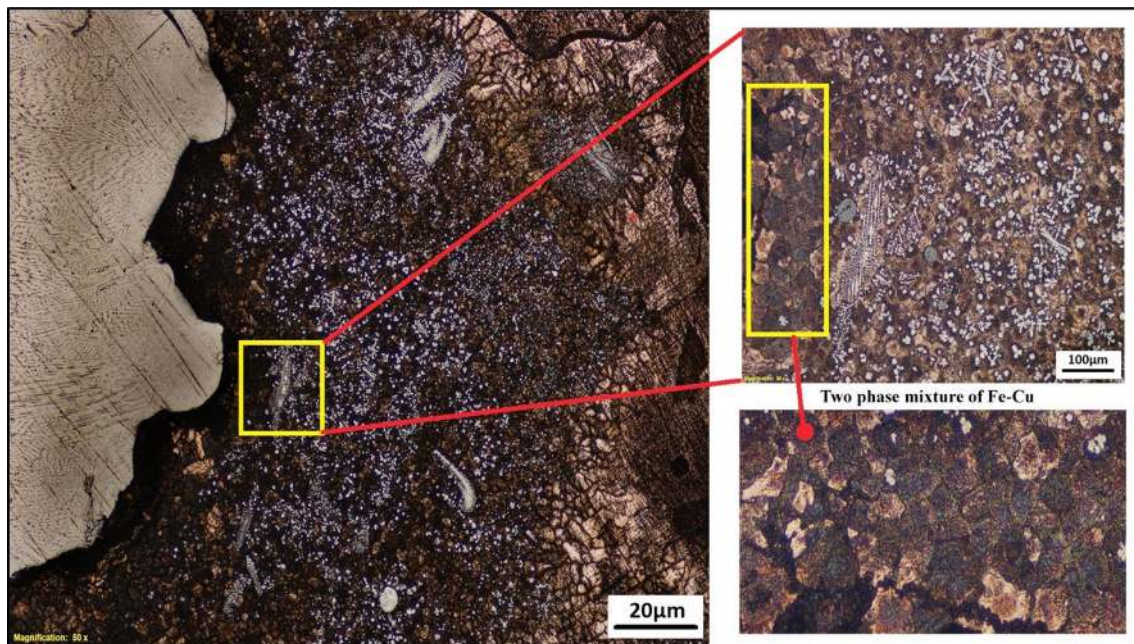


Fig. 5 Fusion zone of SS-316 and copper weld joint

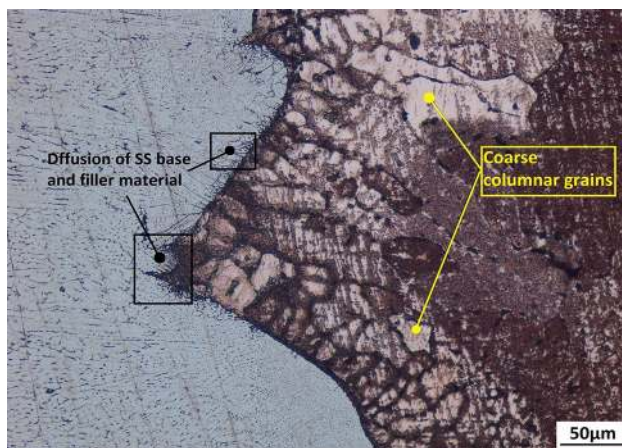


Fig. 6 Microstructure at the weld interface of SS-316 and Copper

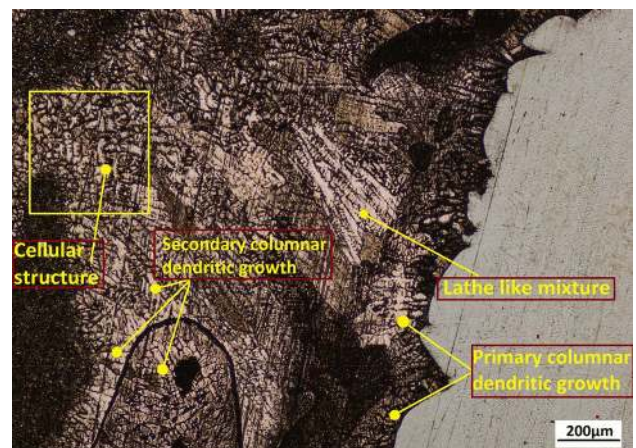


Fig. 7 Optical micrograph of SS-316 and copper showing different grain structures at the weld bead

Hardness and Tensile Test

Micro-indentations were taken along the cross section of the weld bead as marked in Fig. 9. By analyzing the hardness values taken at the weld face and root of the weld shows more inhomogeneity at the top, where copper content is higher. This inhomogeneity can be attributed to the differential cooling rate at the FZ. Due to high thermal conductivity, copper cools at a faster rate than the steel. Hence, inconsistent microhardness distribution at the top surface of FZ revealed higher hardness at the Fe-rich zones. In contrast, lower hardness values were noted at the root of the weld.

During the tensile test, it was observed that the point of instability and necking started occurring in the copper zone. However, the weld bead interfaces at both sides remained intact. Finally, the fracture occurred at the copper side; this suggests that the tensile strength, as well as the structural properties of the weld bead, was better than the copper alone. This can also be related to the hardness values, wherein the average microhardness at the copper side was seen to be around 67. But the average hardness values taken at the weld zone was 107. The ultimate tensile strength (UTS) during the tensile test was measured to be 143.7 MPa, which is almost close to the UTS of copper

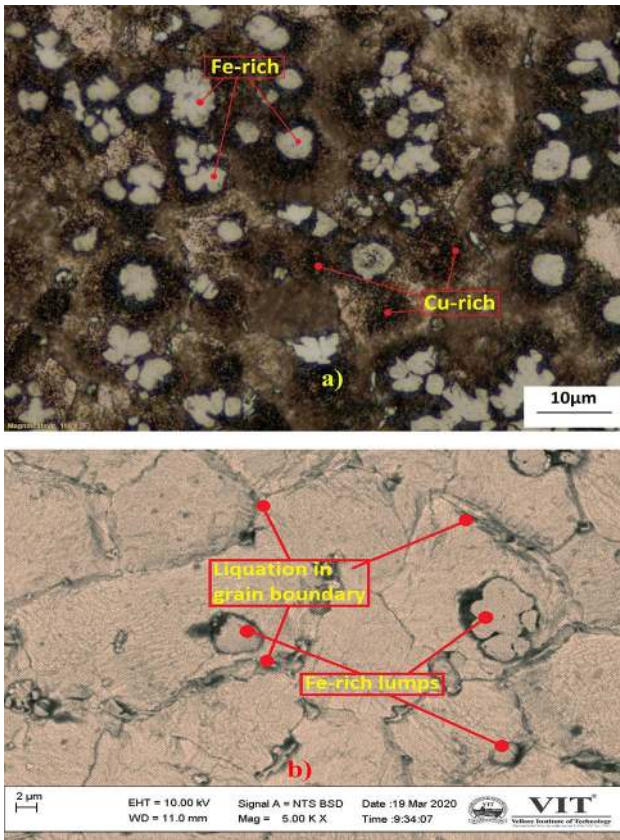


Fig. 8 (a) Optical micrograph at low magnification, and (b) SEM micrograph showing Fe-rich and Cu-rich areas, and liquation grain boundary, respectively, at copper HAZ

with a coarse grain structure due to the prolonged preheating (Table 3).

Conclusions

Based upon the investigation to weld SS-316 and Cu, the following are concluded:

- (1) 316 stainless steel and 99.9% pure copper plates of 5 mm thickness are successfully joined by TIG welding. The microstructure of the joint mainly consists of coarse grain structure at the heat-affected zone (HAZ) of copper and acicular type of grain growth at HAZ of SS-316. Also, some coronal shaped SS-316 particles appeared at the FZ of copper.
- (2) The microhardness values obtained along the cross section of weld bead are mostly influenced by the Cu content in the solution. The values were inconsistent at the weld face compared with the weld root.
- (3) The tensile strength of weldment is measured to be 143.7 MPa, the fracture occurred at the copper base metal zone.

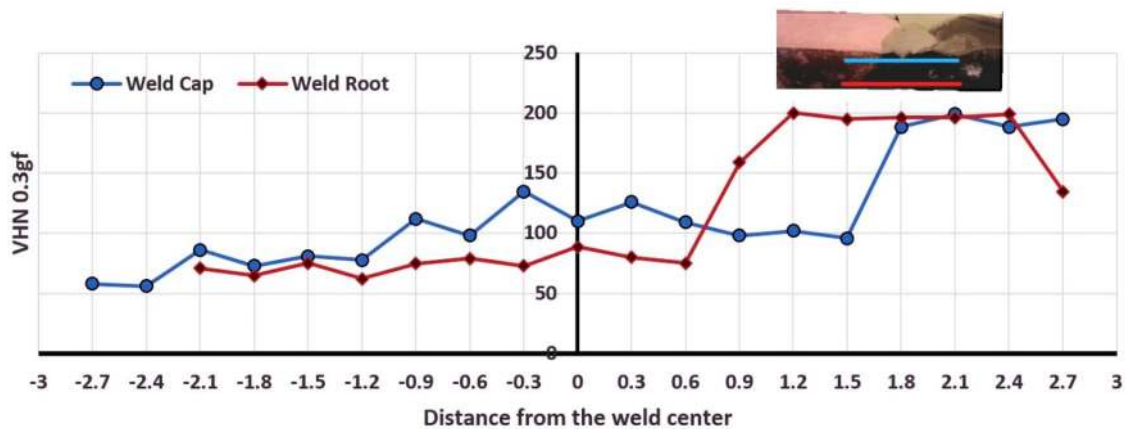


Fig. 9 Microhardness profile along the cross section at weld cap and weld root

Table 3 Mechanical properties of welded material

Material	UTS (MPa)	Yield strength (MPa)
SS-316	480	197
CP-Copper	220	70
ERNiCr-3	450	–

References

- W. Ting, B.G. Zhang, J.C. Feng, Influences of different filler metals on electron beam welding of titanium alloy to stainless steel. *Trans. Nonferrous Met. Soc. China* **24**, 108–114 (2014)
- Z. Sun, R. Karppi, The application of electron beam welding for the joining of dissimilar metals: an overview. *J. Mater. Process. Technol.* **59**, 257–267 (1996)
- P. Taylor, Y.V. Budkin, Welding joints in dissimilar metals. *Weld. Int.* **25**, 523–525 (2011). <https://doi.org/10.1080/09507116.2011.554254>
- A.K. Kadian, P. Biswas, The study of material flow behaviour in dissimilar material FSW of AA6061 and Cu-B370 alloys plates. *J. Manuf. Process.* **34**, 96–105 (2018). <https://doi.org/10.1016/j.jmapro.2018.05.035>
- M. Sarvari, A. Abdollah-zadeh, H. Naffakh-Moosavy, A. Rahimi, Investigation of collision surfaces and weld interface in magnetic pulse welding of dissimilar Al/Cu sheets. *J. Manuf. Process.* **45**, 356–367 (2019)
- P.S. Wei, C. Wen, Missed joint induced by thermoelectric magnetic field in electron-beam welding dissimilar metals—experiment and scale analysis. *Metallur. Mater. Trans. B* **33**, 765–773 (2002)
- M. Kimchi, H. Shao, W. Cheng, P. Krishnaswamy, Magnetic pulse welding aluminium tubes. *Mag. Pul. Wel. Al Tube St.* **48**, 19–22 (2004)
- G.R. Joshi, V.J. Badheka, Processing of bimetallic steel-copper joint by laser beam welding. *Mater. Manuf. Process.* **34**, 1–11 (2019). <https://doi.org/10.1080/10426914.2019.1628262>
- Y. Kaya, G. Eser, Production of ship steel—titanium bimetallic composites through explosive cladding. *Weld. World* **63**, 1547–1560 (2019)
- X. Feng, S. Li, L. Tang, H. Wang, Refill friction stir spot welding of similar and dissimilar alloys: a review. *Acta Metall. Sin. English Lett.* **33**, 30–42 (2020). <https://doi.org/10.1007/s40195-019-00982-4>
- T. Mittler, U. Hofmann, J. Riedle, R. Golle, W. Volk, Fabrication and processing of metallurgically bonded copper bimetal sheets. *J. Mater. Process. Tech.* **263**, 33–41 (2018). <https://doi.org/10.1016/j.jmatprotec.2018.08.008>
- H.-Y. Huang, Effects of shielding gas composition and activating flux on GTAW weldments. *Mater. Des.* **30**, 2404–2409 (2009)
- K. Tseng, C. Hsu, Journal of materials processing technology performance of activated TIG process in austenitic stainless steel welds. *J. Mater. Process. Tech.* **211**, 503–512 (2011). <https://doi.org/10.1016/j.jmatprotec.2010.11.003>
- T.A. Mai, A.C. Spowage, Characterisation of dissimilar joints in laser welding of steel-kovar, copper–steel and copper–aluminium. *Mater. Sci. Eng. A* **374**, 224–233 (2004)
- G.R. Joshi, V.J. Badheka, Studies on tool shoulder diameter of dissimilar friction stir welding copper to stainless steel. *Metallogr. Microstruct. Anal.* **8**, 263–274 (2019). <https://doi.org/10.1007/s13632-019-00532-5>
- B. Zhang, J. Zhao, X. Li, J. Feng, Electron beam welding of 304 stainless steel to QCr0.8 copper alloy with copper filler wire. *Trans. Nonferrous Met. Soc. China.* **24**, 4059–4066 (2014). [https://doi.org/10.1016/S1003-6326\(14\)63569-X](https://doi.org/10.1016/S1003-6326(14)63569-X)
- A. Najafkhani, H. Abbaszadeh, Evaluation of microstructure and mechanical properties of friction stir welded copper / 316L stainless steel dissimilar metals. *Int. J. ISSI* **7**, 21–25 (2010)
- I. Magnabosco, P. Ferro, F. Bonollo, L. Arnberg, An investigation of fusion zone microstructures in electron beam welding of copper—stainless steel. *Mater. Sci. Eng. A* **424**, 163–173 (2006). <https://doi.org/10.1016/j.msea.2006.03.096>
- G.R. Joshi, V.J. Badheka, Microstructures and properties of copper to stainless steel joints by hybrid FSW. *Metallogr. Microstruct. Anal.* **6**, 470–480 (2017). <https://doi.org/10.1007/s13632-017-0398-x>
- G.R. Joshi, V.J. Badheka, Metallographic and microstructure analysis of gas tungsten arc-welded bimetallic copper-to-stainless steel joints. *Metallogr. Microstruct. Anal.* **9**, 180–193 (2020). <https://doi.org/10.1007/s13632-020-00632-7>
- M. Velu, S. Bhat, Metallurgical and mechanical examinations of steel-copper joints arc welded using bronze and nickel-base super-alloy filler materials. *Mater. Des.* **47**, 793–809 (2013). <https://doi.org/10.1016/j.matdes.2012.12.073>
- S.G. Shiri, M. Nazarzadeh, M. Sharifitabar, M.S. Afarani, Gas tungsten arc welding of CP-copper to 304 stainless steel using different filler materials. *Trans. Nonferrous Met. Soc. China* **22**, 2937–2942 (2012). [https://doi.org/10.1016/S1003-6326\(11\)61553-7](https://doi.org/10.1016/S1003-6326(11)61553-7)
- R.P. Shi, C.P. Wang, D. Wheeler, X.J. Liu, Y. Wang, Formation mechanisms of self-organized core/shell and core/shell/corona microstructures in liquid droplets of immiscible alloys. *Acta Mater.* **61**, 1229–1243 (2013). <https://doi.org/10.1016/j.actamat.2012.10.033>
- A. Munitz, Metastable liquid phase separation in tungsten inert gas and electron beam copper/stainless-steel welds. *J. Mater. Sci.* **30**, 2901–2910 (1995)
- C. Roy, V.V. Pavanan, G. Vishnu, P.R. Hari, M. Arivarasu, M. Manikandan, D. Ramkumar, N. Arivazhagan, Characterization of metallurgical and mechanical properties of commercially pure copper and AISI 304 dissimilar weldments. *Procedia Mater. Sci.* **5**, 2503–2512 (2014). <https://doi.org/10.1016/j.mspro.2014.07.502>
- A. Munitz, R. Abbaschian, Liquid separation in Cu-Co and Cu-Co-Fe alloys solidified at high cooling rates. *J. Mater. Sci.* **33**, 3639–3649 (1998). <https://doi.org/10.1023/A:1004663530929>
- Y. Fang, X. Jiang, D. Mo, D. Zhu, Z. Luo, A review on dissimilar metals welding methods and mechanisms with interlayer. *Int. J. Adv Manf. Tech.* **102**, 2845–2863 (2019)

Publisher's Note Springer Nature remains neutral with regard to jurisdictional claims in published maps and institutional affiliations.